Fast sweeping probe system for characterization of spokes in E × B discharges

V. Skoutnev, P. Dourbal, E. Rodríguez, and Y. Raitses

Citation: Review of Scientific Instruments **89**, 123501 (2018); doi: 10.1063/1.5053677
View online: https://doi.org/10.1063/1.5053677
View Table of Contents: http://aip.scitation.org/toc/rsi/89/12
Published by the American Institute of Physics

Fast sweeping probe system for characterization of spokes in E × B discharges

V. Skoutnev,[a] P. Dourbal, E. Rodríguez, and Y. Raitses[b]
Princeton Plasma Physics Laboratory, Princeton University, Princeton, New Jersey 08543, USA

(Received 24 August 2018; accepted 15 November 2018; published online 6 December 2018)

We have developed a rapidly swept, back-to-back 100 kHz Langmuir probe system using a tunable compensating network to study the temporal evolution of low frequency oscillations in Penning discharges, Hall Thrusters, and other E × B discharges. Experimental validation of the probe system is performed at low and high sweeping frequencies in a stable Penning discharge. Then application of the probe system to measurements of plasma parameter fluctuations in a low frequency (4 kHz) rotating spoke and an analysis method using the Hilbert transform are shown. We find that the rotating spoke oscillation conducts approximately a third of the cross field current in our Penning device. *Published by AIP Publishing.* https://doi.org/10.1063/1.5053677

I. INTRODUCTION

Turbulent fluctuations and transient phenomenon are ubiquitous in all laboratory plasmas. A growing need to understand the properties and structure of these phenomena has spurred interest in and development of time resolved Langmuir probe measurements due to their relative simplicity and good spatial resolution. Langmuir probes measure the plasma potential and electron energy distribution function (EEDF) simultaneously based on analysis of the current obtained from sweeping the probe bias voltage. Weighted integration of the EEDF then provides the plasma density and temperature on the time scale at which the probe is swept.[1] The temporal and/or spatial variation of these measurements can then be used to study plasma dynamics such as fluctuation-induced particle and heat transport in fusion devices,[2–4] and coherent oscillatory modes in, for example, Hall thrusters and linear plasma devices.[5–8]

For low sweeping frequencies (around 1 kHz or below), Langmuir probes are typically constructed by connecting a driving voltage source through a small resistor to a metallic end immersed in the plasma. At a given bias voltage, the current collected from the plasma flows through the resistor and can be directly measured. However, at higher sweeping frequencies f of the driving voltage, with peak to peak voltage range V_{pp}, the reactive current $I_R = C\frac{dV}{dt} = \pi f C V_{pp}$ arising from the capacitance C of the coaxial cables (~100 pF/m) and circuitry begins to dominate the true plasma current I_p for $f \gtrsim I_p/(\pi C V_{pp})$ and must somehow be compensated. This is especially relevant for larger plasma devices such as tokamaks, Hall thruster chambers, and linear plasma devices where cables may need to be several meters long. For example, in a typical low temperature plasma measurement at very negative bias voltages where the current is smallest, if the ion saturation current is $I_p \approx I_{sat} \approx 0.5$ mA and a probe system has a net capacitance of 1 nF from ~10 m of cables with a $V_{pp} = 50$ V sweeping voltage range, the reactive current becomes comparable to I_p at around $f = 3$ kHz.

Many solutions to compensate the reactive current have been implemented with varying degrees of success. One idea is to use an additional null probe that runs along the Langmuir probe but is insulated from the plasma so that both have the same capacitance.[3,9–11] The currents through the probes can be separately measured and then subtracted during post-processing to obtain the true plasma current. This approach allows for nearly exact capacitance cancellation between the probes and has been successfully shown to be able to sweep up to 400 kHz in the high-speed dual Langmuir probe system.[12]

Another method consists of using variable capacitors in the internal circuitry of the probe system to simulate and compensate the stray capacitances.[2,4] This method requires calibration at each sweeping frequency but does not require construction of a parallel null probe: the probe system is directly connected to a standard Langmuir probe.

In this article, we describe the design and application of a variable capacitor compensation scheme that allows fast sweep ($f \gtrsim 3$ kHz where $I_R \gtrsim I_{sat}$) measurements. In contrast to previous designs, we measure differential current at low voltages through a particular setup of insulated power amplifiers, avoiding issues with measurements at high sweeping voltages. Section II describes the principle and schematic behind the fast sweep probe system. Section III describes validation of the probe system inside a stable Penning discharge by benchmarking against an accepted commercial probe system, the multifunctional plasma probe analyzer.[13] Section IV describes an application of the fast sweep system to a 4 kHz rotating spoke and an analysis method of the measured fluctuations that implements the Hilbert transform. We find that particle transport due to azimuthal electric field fluctuations across an axial magnetic field contributes to approximately 33% of the anomalous transport in a Penning discharge undergoing spoke oscillations.

II. PROBE SYSTEM ELECTRONICS

The general technique for compensating reactive currents arising from fast sweeping is based on (1) creating a

[a]Electronic mail: vskoutne@pppl.gov
[b]Electronic mail: yraitses@pppl.gov

compensating channel with reactive impedance equivalent to the real probe/chamber system and (2) finding the difference between the current across the created channel and the probe channel to obtain the real plasma current.

A significant difficulty with this approach is the need to resolve the small plasma current (mA) that is the difference between two signals each riding high voltages (±50/100 V) at high frequencies (1-100 kHz). The current measurements at each channel are typically performed across sensing shunts using isolation amplifiers and current meters capable of providing a high dynamic range at the high sweeping frequencies.[12] Amplifiers and current meters satisfying all of the specifications are often either expensive, not commercially available, or prohibitively difficult to construct.

We have implemented a method of creating a compensating channel and measuring differential current free of the above difficulty. By using two (A and B in Fig. 1) fully insulated power amplifiers (including their power supplies), driven with opposite polarities by a common voltage source (C in Fig. 1), we are able to connect their low voltage outputs together at a reference point (D in Fig. 1) grounded to the chamber through a single sensing shunt. For a compensating capacitor calibrated to match the capacitance of the probe channel, the reactive currents in the two channels are identical and the result of analog subtraction (due to the polarity flip of the power amplifiers) at point D leaves only the small plasma current to be measured across the shunt with a single input, low noise amplifier (a demonstration is shown in Appendix A). Since this low noise amplifier is not exposed to the high sweeping voltages, it can have milder specifications and the current meter can have a lower dynamic range to obtain the same sensitivity as a higher dynamic range current meter measuring at high voltages.

Measurement is performed by connecting the low noise amplifier to a PicoScope 5000 series oscilloscope (DAQ in Fig. 1) capable of a sampling rate of 125 MS/s with 14 bit resolution. We use an asymmetric sawtooth waveform for the biasing voltage to provide a uniform distance between samples on the I-V trace and analyze in the region where $\frac{dV}{dt} > 0$, which corresponds to approximately 1000 samples for each single I-V trace at 100 kHz sweeping.

This design allows us to perform measurements of Langmuir I-V traces and their derivatives up to sweeping frequencies of 100 kHz. Calibrating at a given sweeping frequency consists of substituting the Langmuir probe in Fig. 1 with a resistor and adjusting the variable compensating capacitor within its range of $\lesssim$1400 pF until there is no phase lag between applied AC voltage and measured current. The calibration does not account for the additional impedance of the Langmuir probe. The extra capacitance from a Langmuir probe of area A and a typical probe sheath on the order of a Debye length, λ_D, is on the order of $0.5\varepsilon_0 A/\lambda_D \approx 1$ pF, where ε_0 is the vacuum permittivity. This ∼1 pF sheath capacitance is, however, negligible compared to the original ∼1 nF capacitance of the cables and circuitry.

III. PROBE SYSTEM VALIDATION

To validate the accuracy of our probe system across the range of sweeping frequencies 1-100 kHz, we compare experimental measurements in a stable Penning discharge against the Multifunctional Plasma Probe Analyzer (MFPA) developed by Plasma Sensors, a tested and accepted commercial probe system that provides high energy resolution and dynamic range EEDF measurements.[13] The MFPA uses a reference probe to eliminate distortions associated with floating potential fluctuations and typically averages ≥100 sweeps at 1 kHz to produce robust I-V traces.

We setup a stable (no large plasma oscillations present) argon Penning discharge at 1.5 mTorr with a crossed radial electric and 30 G axial magnetic field, corresponding to an electron gyroradius of $\rho_g \approx 1$ mm. A cylindrical, tungsten Langmuir probe (diameter $d_p = 0.1$ mm and length 3 mm) is placed perpendicular to the magnetic field where beam effects are not present and an isotropic, near-Maxwellian electron population is present.[14] A few gyroradii outside ($10\rho_g \approx 1$ cm) the axis-centered beam, isotropy is maintained primarily by electron-neutral collisions with a mean free path of 50 cm and collision frequency of 0.5 MHz, much faster than the 4 kHz spoke oscillations. The Langmuir probe is biased relative to the metal walls of the chamber, which have large enough area to compensate for the current flowing into the

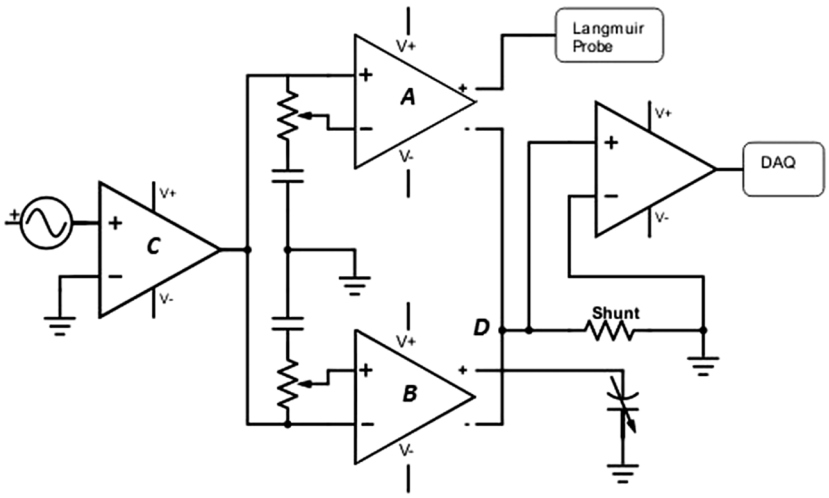

FIG. 1. Electronic schematic of the main components of the fast sweep probe system. Point D is where reactive currents undergo analog subtraction due to their inverted input voltage signals and the remaining plasma current is measured across the shunt using a low noise amplifier in parallel.

probe. Note that although electrons are magnetized, we may still apply conventional probe theory for non-magnetized plasmas because the ratio of the probe radius to the gyroradius $\frac{d_p}{2\rho_g} \approx 0.05$ is small.[15,16]

For the validation experiment, at each sweeping frequency of the fast sweep probe system (FSPS), 10 sets of 50 back-to-back I-V traces are taken followed by the recording of an identical number of traces at 1 kHz using MFPA on the same Langmuir probe. Alternating between probe systems accounts for any drifts in the discharge on the time scale of minutes over the course of the experiment (recalibration of FSPS for each frequency takes a few minutes).

To compute the plasma potential and the EEDF from the data sets, we implement the Druyvesteyn method for isotropic energy distributions.[16,17] The EEDF has been shown to be the most reliable probe diagnostic for low temperature laboratory and processing plasmas.[18] The Druyvesteyn method starts with taking the second derivative of the plasma current $I(V)$ with respect to the bias voltage and finding the plasma potential V_p from where $I''(V) = 0$. The EEDF $F(\varepsilon)$ and the related electron energy probability function (EEPF) $f_p(\varepsilon) = F(\varepsilon)/\sqrt{\varepsilon}$ are then given by the Druyvesteyn formula,[16]

$$\frac{d^2I}{d^2V} = -\frac{e^2S_p}{4}\sqrt{\frac{2e}{\mathrm{mV}}}F(\mathrm{eV}) = \frac{e^3S_p}{2\sqrt{2m}}f_p(\mathrm{eV}), \tag{1}$$

where S_p is the probe area, e is the electron charge, m is the electron mass, and $V \le 0$ is taken to be relative to V_p. The plasma density and effective temperature are then found by integration of the EEDF,[16]

$$N = \frac{2\sqrt{2m}}{|e|S_p}\int_0^{-\infty} I''(V)\sqrt{V/e}\,dV, \tag{2}$$

$$T_e = \frac{4\sqrt{2m/|e|}}{3NS_p}\int_0^{-\infty} I''(V)|V|^{\frac{3}{2}}dV. \tag{3}$$

For $f_{\mathrm{sweep}} \lesssim f_{\mathrm{pi}} \approx 10^6$ Hz (the ion plasma frequency), collisionless, thin sheath theory holds and polarization and sheath capacitance effects are negligible.[19] 100 kHz is safely within this limit, so any variations in the measured plasma parameters with increasing sweeping frequency are an effect of the probe system electronics, analysis technique, errors in calibration, and drifts in the discharge between measurements.

We find that measured plasma parameters (Fig. 2) with the two probe systems have relative differences of around 10%–20%, whose origin can be seen in the comparison of four representative EEPFs in Fig. 3. Note that the peaks of all the EEPFs occur between 1.5 and 2 eV, which is less than half the average measured temperature $T_e \approx 4$ eV of the discharge and therefore satisfies the criterion for acceptable EEPF measurements given by Godyak.[16] In the lower energy range $\lesssim 2T_e$, where the majority of the electron population resides, the $f_{\mathrm{p,FSPS}}^{100\ \mathrm{kHz}}$ is larger, while $f_{\mathrm{p,FSPS}}^{1\ \mathrm{kHz}}$ is smaller than $f_{\mathrm{p,MFPA}}^{1\ \mathrm{kHz}}$. This corresponds to the relatively higher and lower measured density, respectively, seen in Fig. 2. The difference in temperature measurements occurs due to different

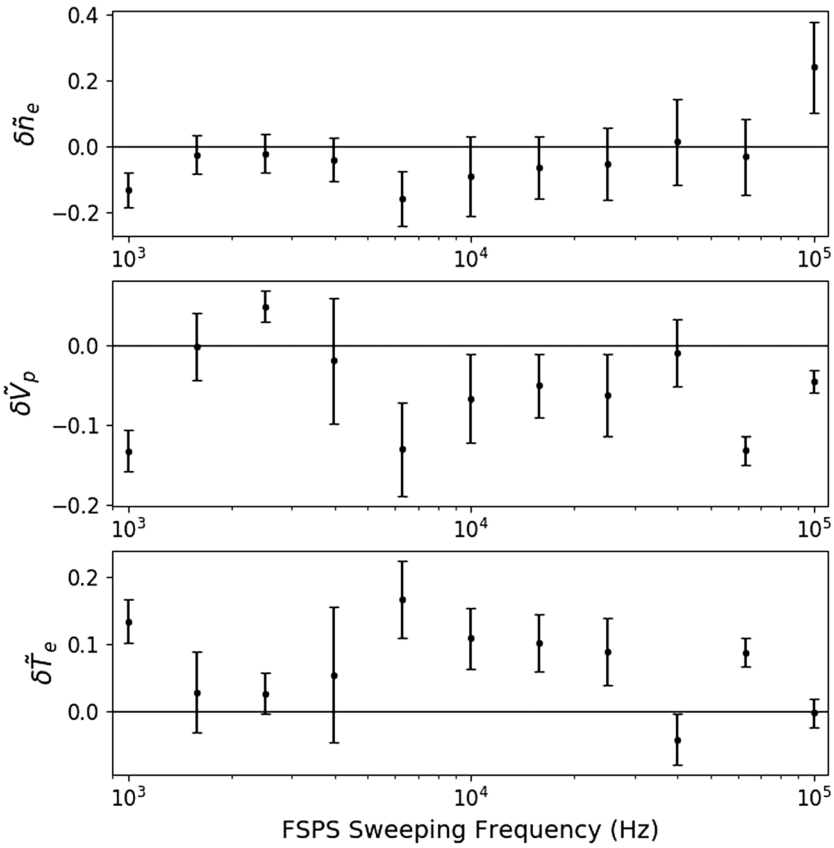

FIG. 2. Relative errors (e.g., $\delta\tilde{n}_e = \frac{\delta n_e}{n_e}$) between FSPS and MFPA are shown versus sweeping frequency of FSPS: δ in density (top), plasma potential (middle), and temperature (bottom). MFPA control measurements are always taken at 1 kHz. The mean and standard deviation (error bars) are computed from 10 sets of 50 measured plasma parameters at each FSPS sweeping frequency.

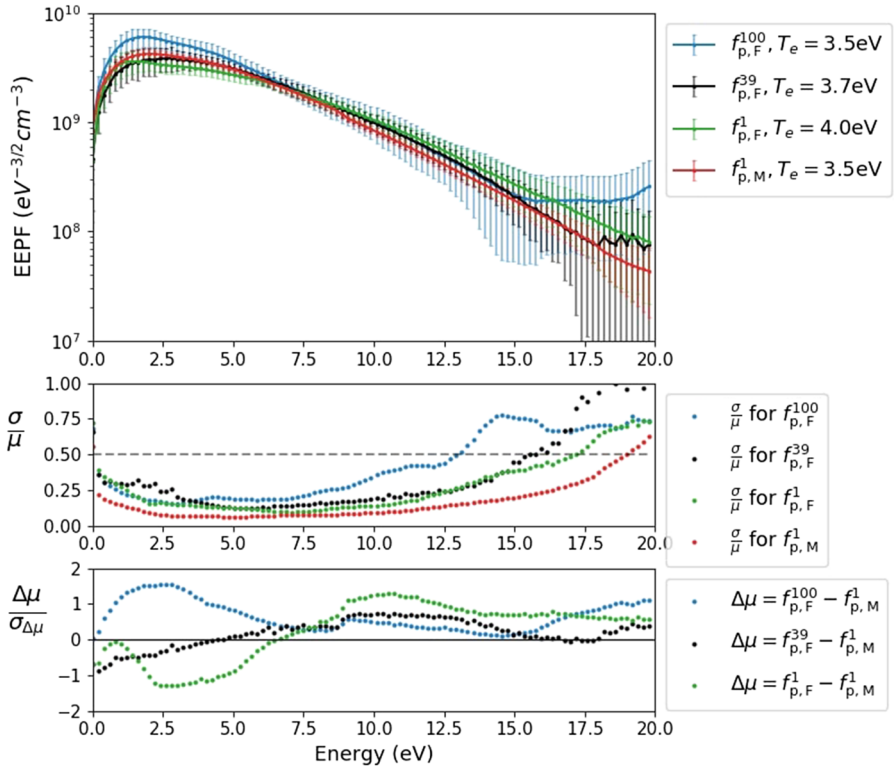

FIG. 3. Top: Average EEPFs computed by binning the EEPFs from one set of 50 I-V traces for three representative FSPS sweeping frequencies (1 kHz, 39 kHz, and 100 kHz corresponding to $f^{1}_{p,F}$, $f^{39}_{p,F}$, and $f^{100}_{p,F}$, respectively) and the MFPA at 1 kHz ($f^{1}_{p,M}$) taken during the 10 kHz experiment (see Appendix B for I-V traces). Error bars are the standard deviation of the energy bins containing values from the 50 individual EEPFs. Middle: The coefficient of variation for each of the EEPFs where $\mu(\varepsilon)$ and $\sigma(\varepsilon)$ are the mean and standard deviation of the energy bins. Bottom: The reciprocal coefficient of variation of the difference between FSPS and MFPA EEPFs.

slopes of the EEPFs ($\log(f_p(\varepsilon)) \propto -1/T_e$). From the top and bottom panels of Fig. 3, it is roughly visible that $f^{1\text{ kHz}}_{p,FSPS}$ has a smaller average slope, while $f^{100\text{ kHz}}_{p,FSPS}$ has a similar average slope compared to the slope of $f^{1\text{ kHz}}_{p,MFPA}$, corresponding to the relatively higher and similar measured effective temperature, respectively, seen in Fig. 2. $f^{39\text{ kHz}}_{p,FSPS}$ is quantitatively similar to $f^{1\text{ kHz}}_{p,FSPS}$.

At higher energies $\varepsilon \gtrsim 3T_e$, the coefficient of variation rises above $\frac{\sigma}{\mu} = 0.5$ at $4.4T_e$, $4.7T_e$, and $3.7T_e$ for $f^{1\text{ kHz}}_{p,FSPS}$, $f^{39\text{ kHz}}_{p,FSPS}$, and $f^{100\text{ kHz}}_{p,FSPS}$, respectively, where $\mu(\varepsilon)$ and $\sigma(\varepsilon)$ are the mean and standard deviation of the energy bins. We choose $\frac{\sigma}{\mu} = 0.5$ as the cutoff above which probe system distortions and electronic noise become too significant for analysis and therefore we restrict EEPF analysis to energy ranges $\varepsilon_{max} \lesssim 3.7T_e \approx 13$ eV in future measurements at higher sweeping frequencies. Analysis of other sweeping frequencies shows that ε_{max} is roughly unchanged below 39 kHz and begins to decrease for higher frequencies.

The coefficient of variation ($\frac{\sigma}{\mu}$) of MFPA is lower than that of FSPS over the whole energy range because MFPA has lower internal electronic noise than FSPS due to the roughly 100 times higher frequency bandwidth of FSPS's measurement instruments. Sweeping across a resistor, we find that MFPA has an internal electronic noise floor of around 7 μA, while the FSPS's is around 200 μA, independent of the sweeping frequency. The higher noise floor interferes with resolution of the ion saturation regime and therefore the high energy tail of the EEPF. Density and effective temperature integrals are fortunately primarily determined by the much larger lower energy electron population, limiting the effects of a higher noise floor. This allows FSPS measurements to maintain a relative error within 20% of the low frequency 1 kHz MFPA measurements while sweeping across two orders of magnitude higher frequencies.

Overall, sweeping the FSPS at higher frequency leads to both over- and underestimation of plasma parameters and to a decrease in the highest resolved energy. Relative differences within 20% between FSPS and MFPA measurements in a quiescent plasma give us confidence to extend the probe system to study plasma parameter variations in a non-stationary plasma.

IV. MEASUREMENTS IN A ROTATING SPOKE

The Penning discharge also has a non-stationary state where a robust azimuthally rotating spoke with mode number m = 1 is present, analogous to the higher mode number spokes found in Hall thrusters.[14,20–22] Spokes have been linked to anomalous transport in Hall thrusters and known to reduce thruster efficiency.[21,22] Penning discharges and Hall Thrusters often require an effective electron collision frequency 10^2–10^3 times larger than the classical electron-atom collision frequency to match measurements of the cross field transport, necessitating the presence of other physical mechanisms to explain the enhanced transport.[22–25] Characterizing the correlations between the fluctuating plasma parameters can help determine the driving factors behind the anomalous transport.[26]

We setup a xenon Penning discharge at 0.1 mTorr with a 40 G magnetic field, experimental conditions for which the spoke is present and has a rotation frequency of approximately 4 kHz. The Langmuir probe is placed at a fixed

location and swept with the FSPS at 50 kHz (sufficiently above the Nyquist frequency of the spoke), obtaining a time series of plasma parameter measurements as shown in Fig. 4.

Due to the turbulent nature of the spoke, we attempt to statistically capture the azimuthal distribution of the plasma parameters. The general approach is to extract the instantaneous phase of each plasma parameter relative to the spoke oscillation (defined by the density oscillation in this paper) from the Hilbert transform of its time series and then construct the azimuthal profile by binning over many spoke periods. Hilbert transforms have been applied in experimental plasma data previously, both for fusion devices[27–29] and Hall thrusters.[30,31] Temporal variation of the amplitude and frequency of a spoke mode makes nonstationary signal analysis more effective than standard Fourier techniques because it can track instantaneous variation of the amplitude and phase of a given mode.[32] The Hilbert transform requires a signal with one dominant oscillatory mode, which makes its application to studying breathing and spoke modes in E × B discharges particularly amenable.

The Hilbert transform $\widetilde{D}(t)$ of the density time series $D(t)$ results in an analytic signal of the form

$$S_D(t) = D(t) + i\widetilde{D}(t) = A_D(t)e^{i\theta_D(t)}, \tag{4}$$

where $A_D(t)$ is a slow varying envelope and $\theta_D(t)$ is the fast varying instantaneous phase with $\partial_t\theta_D \approx 4$ kHz for our spoke. We choose the instantaneous phase $\theta_D(t) = \arg(S_D(t))$ of the density as the reference phase of the spoke oscillation (i.e., the peak in density corresponds to $\theta = 0$). Statistics of the phases of the plasma potential and temperature relative to the spoke density can then be studied either by taking temporal averages of $\theta_P(t) - \theta_D(t)$ and $\theta_T(t) - \theta_D(t)$, respectively, or by analyzing the final phase plots. An example of the resulting phase plot after binning ~40 spoke periods (10 ms) is shown in Fig. 5, and a few representative phase binned EEPFs are plotted in Fig. 6 for reference. Compared to the EEPFs in a stationary discharge (Fig. 3), the turbulent variation in the spoke itself between periods and increased plasma noise during individual I-V trace measurements leads to a larger variation of EEPFs at a given phase (larger error bars) and smoother EEPFs (due to the need for stronger filtering), respectively.

It is important to note that bandpass filtering the data may be necessary prior to applying the Hilbert transform and binning. A lowpass filter allows the Hilbert transform to pick out the low frequency spoke oscillation of interest from any high frequency oscillations or noise. A highpass filter removes slow variations in the mean value of the time series which would uniformly increase the error bars in the phase plot. The bandpass window should be chosen around the primary frequency and increased until either of the two effects begins to distort the phase plot. The phase plot in Fig. 5 uses two second order Bessel filters, one with a lowpass cut-off frequency of 10 kHz and the other with a highpass cut-off frequency of 1 kHz.

An estimate of anomalous transport due to radial $E \times B$ transport can be made directly from the phase plot. Variation of the plasma potential azimuthally results in an $E_\phi = \frac{1}{R}\frac{dV}{d\phi}$ which causes radial $v_{E\times B} = \vec{E} \times \vec{B}/B^2$ transport due to the axial magnetic field. Under the assumption that the spoke is

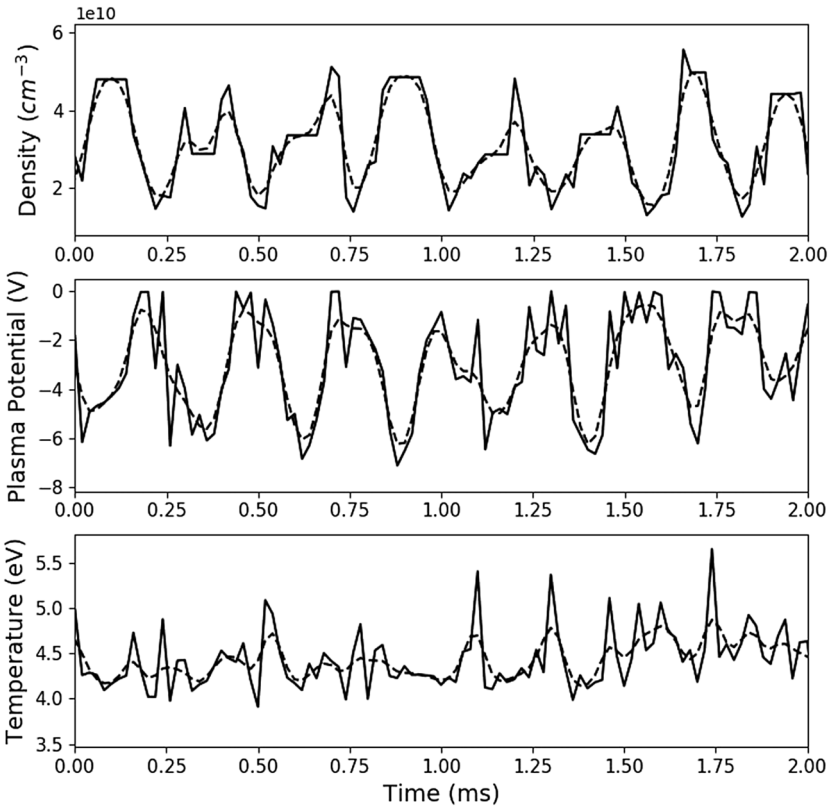

FIG. 4. A sample 2 ms time series of FSPS measurements. Each point is one voltage sweep. The underlying dashed curve is the result of a 2nd order lowpass Bessel filter at a cut-off frequency of 10 kHz.

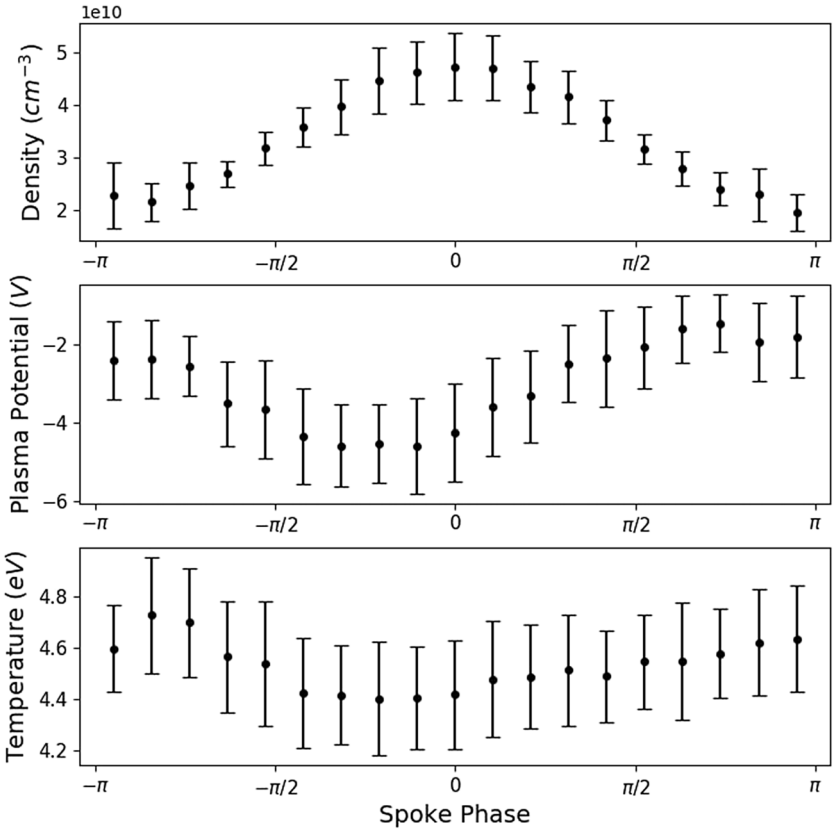

FIG. 5. Azimuthal profiles of plasma parameters inside the spoke determined from binning the filtered plasma parameter time series according to the instantaneous phase of the Hilbert transform of the density time series. Error bars are the standard deviations of the bins.

rigidly rotating over the time scale of its period, the probe time series measurement is translated to azimuthal variation by $\phi = \theta_D(t)$. With the Langmuir probe at a distance $R = 4$ cm in our cylindrical Penning discharge of length $L = 38$ cm, we approximate the azimuthal variation to be sinusoidal ($\delta \mathrm{n}(t) = \delta \mathrm{n} \cos(\theta_D(t))$, $\delta \mathrm{V}(t) = \delta \mathrm{V} \cos(\theta_\mathrm{D}(t) + \theta_{\delta \mathrm{n}, \delta \mathrm{V}})$) to estimate the total anomalous radial current,

$$\mathrm{I_a} = \langle e n v_{E\times B} \rangle 2\pi R L = -\frac{e\pi L}{B} \delta \mathrm{n} \delta \mathrm{V} \sin(\theta_{\delta \mathrm{n}, \delta \mathrm{V}}). \quad (5)$$

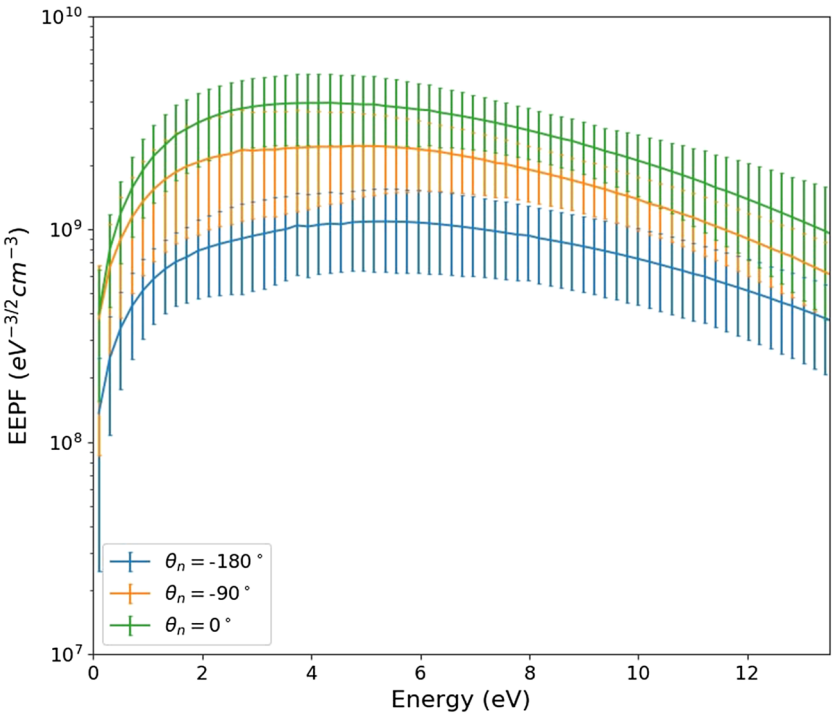

FIG. 6. Representative EEPFs at different phases of the spoke density oscillation. EEPFs are restricted below $3T_e \approx 13.5$ eV.

Equation (5) gives $I_a = 0.4$ A when taking values $\delta n \approx 1.1 \times 10^{10}$ cm^{-3}, $\delta V \approx 1.1$ V, and $\theta_{\delta n,\delta V} \approx -\frac{\pi}{4}$ from the phase plot. This anomalous current is 33% of the total measured discharge current of 1.2 A, revealing the potentially important role the spoke plays in cross field transport. Previous experiments in Hall thrusters have found a spoke contribution of 50%[33] or more,[23] largely consistent with our result. Further study of radial variation and a separate independent measurement of the phase $\theta_{\delta n,\delta V}$ are necessary to constraint the contribution of the spoke to anomalous transport in the oscillatory mode of the Penning discharge. Such experimental and related simulation studies are underway.

V. CONCLUSION

We have demonstrated the implementation of a fast sweeping Langmuir probe system that uses fully insulated power amplifiers (including their power supplies) to allow for analog subtraction of reactive and probe currents and thus direct measurement of the plasma current at low voltages. The probe system was shown to provide EEDF, density, plasma potential, and temperature measurements at sweeping frequencies up to 100 kHz to within 20% of measurements with MFPA, a well accepted probe system in the field capable of obtaining robust I-V traces at low sweeping frequencies of 1 kHz and below.[13,16]

In an application of the probe system, an analysis procedure of time series data of a 4 kHz oscillatory mode in a Penning discharge using the Hilbert transform was presented. The generated phase plot using the Hilbert transform approach gives a clear picture of the average magnitude of fluctuations of the plasma parameters and their mutual phase differences for a dominant mode in an $E \times B$ discharge. This allowed for an estimation of particle transport due to azimuthal electric field fluctuations which showed that a rotating spoke contributes approximately 33% of the anomalous transport in a Penning discharge undergoing spoke oscillations.

ACKNOWLEDGMENTS

The authors are indebted to Alex Merzhevskiy for engineering support on probe systems and the Penning device. We are grateful to Igor Kaganovich, Ivan Romadanov, and Andrei Smolyakov for discussions on spoke phenomenon. Thanks also to Valery Godyak and Benjamin Alexandrovich for support on operation of MFPA.

This work was supported by the Air Force Office of Scientific Research (AFOSR).

APPENDIX A: COMPENSATION DEMO

To demonstrate the principle behind the compensation network, we show the result of measurement using FSPS of the current from a R = 3.3 kΩ resistor driven at 50 kHz with a 10 V amplitude sine wave offset by +10 V. The top panel of Fig. 7 shows opposite polarities of the driving voltage going into amplifiers A and B of Fig. 1. The bottom panel shows the measured I-V curve for the resistor when the compensating capacitor is either set to 0 (no compensation) or is calibrated (with compensation). As expected, compensating the capacitance of the cables leads to the I-V trace of a resistor with $I = V/R$.

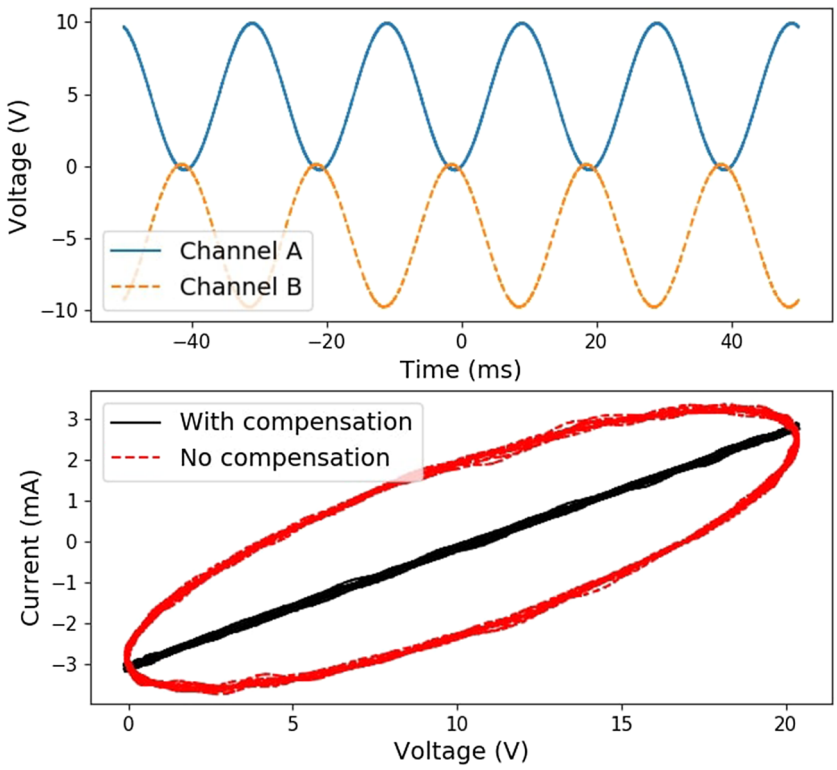

FIG. 7. Top: Shown are the voltage inputs into amplifiers A and B in Fig. 3 when the driving signal at C is a 10 V amplitude sine wave with a +10 V offset. Bottom: The I-V curve for a 3.3 kΩ resistor in place of the Langmuir probe with and without a compensating capacitance.

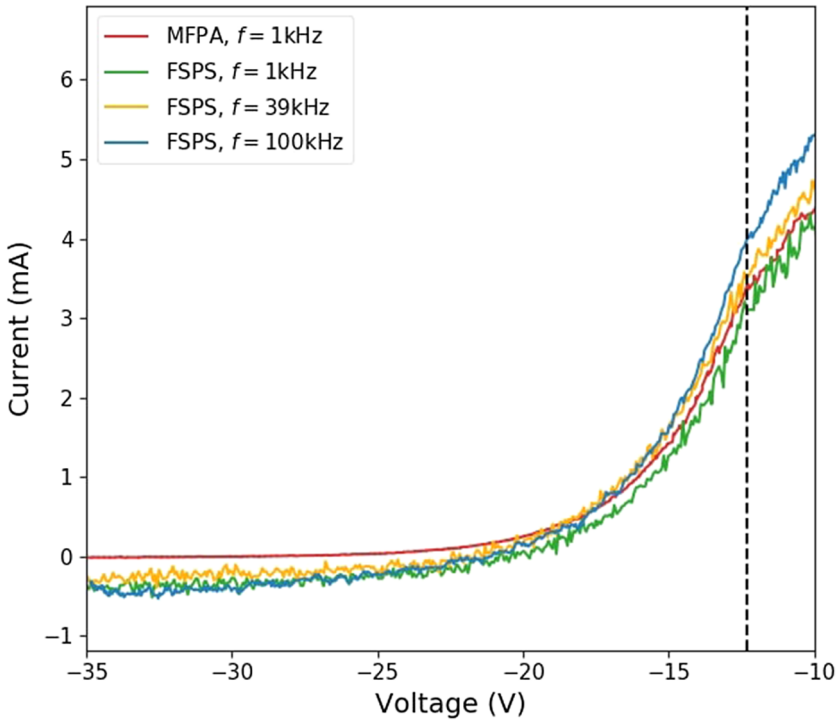

FIG. 8. I-V traces corresponding to the EEPFs in Fig. 3 during the validation experiment for different probe systems and sweeping frequencies. Dashed vertical line is located at the plasma potential.

APPENDIX B: I-V TRACES

We include I-V traces corresponding to the EEPFs in the validation experiment (Sec. III) for reference. Each I-V trace in Fig. 8 is the average of one set of 50 traces. Variation in the electron saturation current region near the plasma potential is normal in a discharge. However, at lower bias voltages, FSPS struggles to resolve the small ion current due to its larger internal noise, leading to the deviations of the MFPA and FSPS EEPFs at higher energies in Fig. 3 ($\gtrsim$13 eV on the EEPFs corresponds to $\lesssim -25$ V on the I-V traces).

[1] J. D. Swift and M. J. R. Schwar, *Electrical Probes for Plasma Diagnostics* (Iliffe Books, London, 1970).
[2] M. Schubert, M. Endler, and H. Thomsen, Rev. Sci. Instrum. **78**, 053505 (2007).
[3] L. Giannone, R. Balbín, H. Niedermeyer, M. Endler, G. Herre, C. Hidalgo, A. Rudyj, G. Theimer, and P. Verplanke, Phys. Plasmas **1**, 3614 (1994).
[4] P. C. Liewer, J. M. Mcchesney, S. J. Zweben, and R. W. Gould, Phys. Fluids **29**, 309 (1986).
[5] E. Chesta, C. Lam, N. Meezan, D. Schmidt, and M. Cappelli, IEEE Trans. Plasma Sci. **29**, 582 (2001).
[6] M. Sekerak, M. Mcdonald, R. Hofer, and A. Gallimore, in *2013 IEEE Aerospace Conference* (IEEE, 2013).
[7] E. Wallace, E. Thomas, A. Eadon, and J. D. Jackson, Rev. Sci. Instrum. **75**, 5160 (2004).
[8] W. Gekelman, H. Pfister, Z. Lucky, J. Bamber, D. Leneman, and J. Maggs, Rev. Sci. Instrum. **62**, 2875 (1991).
[9] G. Chiodini, C. Riccardi, and M. Fontanesi, Rev. Sci. Instrum. **70**, 2681 (1999).
[10] F. F. Chen, in *Plasma Diagnostic Techniques*, edited by R. H. Huddlestone (Academic, New York, 1965).
[11] T. F. Yang, Q. X. Zu, and P. Liu, Rev. Sci. Instrum. **66**, 3879 (1995).
[12] R. B. Lobbia and A. D. Gallimore, Rev. Sci. Instrum. **81**, 073503 (2010).
[13] See http://www.plasmasensors.com/ for MFPA Probe System.
[14] Y. Raitses, I. Kaganovich, and A. Smolyakov, in 2015 International Electric Propulsion Conference, 2015.
[15] Y. M. Kagan and V. I. Perel, Sov. Phys.-Usp. **6**, 767 (1964).
[16] V. A. Godyak and V. I. Demidov, J. Phys. D: Appl. Phys. **44**, 233001 (2011).
[17] M. J. Druyvesteyn and F. M. Penning, Rev. Mod. Phys. **12**, 87 (1940).
[18] V. A. Godyak and B. M. Alexandrovich, J. Appl. Phys. **118**, 233302 (2015).
[19] R. B. Lobbia and A. D. Gallimore, Phys. Plasmas **17**, 073502 (2010).
[20] Y. Sakawa, C. Joshi, P. K. Kaw, F. F. Chen, and V. K. Jain, Phys. Fluids B **5**, 1681 (1993).
[21] J. A. Carlsson, I. D. Kaganovich, A. V. Khrabrov, A. Smolyakov, D. Sydorenko, and Y. Raitses, in *2015 IEEE International Conference on Plasma Sciences (ICOPS)* (IEEE, 2015).
[22] J. Carlsson, I. Kaganovich, A. Powis, Y. Raitses, I. Romadanov, and A. Smolyakov, Phys. Plasmas **25**, 061201 (2018).
[23] C. L. Ellison, Y. Raitses, and N. J. Fisch, Phys. Plasmas **19**, 013503 (2012).
[24] C. Boniface, L. Garrigues, G. J. M. Hagelaar, J. P. Boeuf, D. Gawron, and S. Mazouffre, Appl. Phys. Lett. **89**, 161503 (2006).
[25] J. B. Parker, Y. Raitses, and N. J. Fisch, Appl. Phys. Lett. **97**, 091501 (2010).
[26] A. T. Powis, J. A. Carlsson, I. D. Kaganovich, Y. Raitses, and A. Smolyakov, Phys. Plasmas **25**, 072110 (2018).
[27] A. M. Kakurin and I. I. Orlovsky, Plasma Phys. Rep. **30**, 370 (2004).
[28] R. Jha, D. Raju, and A. Sen, Phys. Plasmas **13**, 082507 (2006).
[29] E. D. Taylor, C. Cates, M. E. Mauel, D. A. Maurer, D. Nadle, G. A. Navratil, and M. Shilov, Rev. Sci. Instrum. **70**, 4545 (1999).
[30] J. Kurzyna, S. Mazouffre, A. Lazurenko, L. Albarède, G. Bonhomme, K. Makowski, M. Dudeck, and Z. Peradzyński, Phys. Plasmas **12**, 123506 (2005).
[31] J. Vaudolon and S. Mazouffre, Plasma Sources Sci. Technol. **24**, 032003 (2015).
[32] R. N. Bracewell, *The Fourier Transform and its Applications* (McGraw-Hill, New York, 1988).
[33] M. Mcdonald, C. Bellant, B. S. Pierre, and A. Gallimore, in *47th AIAA/ASME/SAE/ASEE Joint Propulsion Conference and Exhibit* (AIAA, 2011).